Metrologia

Electron paramagnetic resonance study of silicon-28 single crystal for realization of the kilogram

To cite this article: Shigeki Mizushima and Takahide Umeda 2022 *Metrologia* **59** 025005

OPEN ACCESS
IOP Publishing | Bureau International des Poids et Mesures Metrologia

Metrologia **59** (2022) 025005 (13pp) https://doi.org/10.1088/1681-7575/ac5584

Electron paramagnetic resonance study of silicon-28 single crystal for realization of the kilogram

Shigeki Mizushima[1,2,*] **and Takahide Umeda**[1]

[1] Institute of Applied Physics, University of Tsukuba, 1-1-1 Tennodai, Tsukuba, Ibaraki 305-8573, Japan
[2] National Metrology Institute of Japan NMIJ, 1-1-1 Umezono, Tsukuba, Ibaraki 305-8563, Japan

E-mail: s.mizushima@aist.go.jp

Received 7 December 2021, revised 11 February 2022
Accepted for publication 15 February 2022
Published 14 March 2022

Abstract

To realize the kilogram with high accuracy using the x-ray crystal density method, mass deficit correction to account for the number of vacancy defects in silicon-28 crystals is necessary. In this paper, we present the results of electron paramagnetic resonance (EPR) spectroscopy experiments performed on a silicon-28 crystal. The crystal was cut from near the radial center of the Si28–23Pr11 crystal boule where a relatively high vacancy defect concentration was expected within the boule, which was grown by the floating zone method. We obtained both the in-phase and out-of-phase EPR spectra, which focused on the fast- and slow-spin relaxation centers, respectively. Based on EPR measurements both in the dark and under illumination, the concentrations of phosphorus impurities with unpaired electrons were found to be between 1.6×10^{12} cm^{-3} and 3.4×10^{12} cm^{-3}. In contrast, EPR-active vacancy defects in the silicon-28 crystal were not detected at the detection sensitivity of the present measurements (around 1×10^{12} cm^{-3}), although at the Si/SiO_2 interface, dangling-bond defects (P_{b0} centers) were detected with an areal density between 0.4×10^{12} cm^{-2} and 1.7×10^{12} cm^{-2}. The experimental detection of a larger amount of phosphorus donors under illumination indicates the presence of compensation centers (electronic levels acting as acceptors) with a concentration of at most 1.6×10^{12} cm^{-3}. We determined that such a concentration is mainly compensated by the boron acceptors, and that there is little contribution of electrically active vacancy defects, $0.0(6) \times 10^{12}$ cm^{-3}. This value is much smaller than the previously reported concentrations of 1×10^{14} cm^{-3} to 4×10^{14} cm^{-3} for vacancy defects determined by positron annihilation spectroscopy.

Keywords: kilogram, x-ray crystal density method, silicon-28, vacancy defects, electron paramagnetic resonance

(Some figures may appear in colour only in the online journal)

* Author to whom any correspondence should be addressed.

1. Introduction

The kilogram is the unit of mass in the International System of Units and had been defined based on the mass of an artifact, the International Prototype of the Kilogram (IPK), since 1889. To ensure the long-term stability of the unit of mass, the 26th meeting of the General Conference on Weights and Measures approved the kilogram to be redefined by the realization experiments by fixing the value of the Planck constant h to 6.626 070 15×10^{-34} J s in November 2018 [1]. The redefinition took effect from May 20, 2019.

At present, there are two independent methods officially recognized as primary methods by the Consultative Committee for Mass and Related Quantities (CCM) for realizing the definition of the kilogram with the highest accuracy [2]. In the first method, an electromechanical balance, such as a Kibble balance or a joule balance, is used. The second method is the x-ray crystal density (XRCD) method, in which the kilogram is realized by counting the number of atoms in a crystal.

To date, two international comparisons on the realization of the kilogram by national metrology institutes and the Bureau International des Poids et Mesures have been conducted. The first is the CCM.R-kg-P1 pilot study conducted before the redefinition in which the consistency and continuity of the unit of the mass after the redefinition was confirmed [3]. The relative standard uncertainty of the weighted mean of the five realization experiments was 1.0×10^{-8}. The second comparison is the CCM.M-K8.2019 key comparison carried out after the redefinition in which the key comparison reference value (KCRV) was determined as the weighted mean of seven realization experiments [4]. The relative standard uncertainty of the KCRV was 7.5×10^{-9}. Along with the data directly traceable to the IPK, the results of these two international comparisons provided inputs for the calculation of the consensus value for the international coordination of the dissemination of the kilogram [5].

The XRCD method, which uses silicon-28 crystals, has been under development by the International Avogadro Coordination Project since 2004 [6]. To realize the kilogram using the XRCD method, the number of atoms contained in a single-crystal silicon-28 sphere with a diameter of approximately 93.7 mm is counted by measuring its volume and lattice constant. If the crystal contains vacancy defects, the estimated number of atoms counted from the volume and lattice constant will be larger than the actual number of atoms. Therefore, a mass deficit correction must be applied to account for the number of vacancy defects in the crystal in the XRCD method.

To date, the vacancy defect concentration in silicon crystals has been measured for the purpose of determining the mass deficit correction with microgram-level uncertainty using positron annihilation spectroscopy (PAS) [7, 8]. At present, the result of PAS is adopted for the mass deficit correction in the XRCD method.

To verify the reliability of this mass deficit correction, vacancy defect concentration has been measured by another independent method, electron paramagnetic resonance (EPR) [9, 10]. The samples used in the EPR studies were extracted from more than 15 mm from the radial center of the crystal boule. Only the in-phase spectra at the microwave power $p = 2$ mW were presented in those studies.

This paper presents the latest EPR results for a silicon-28 crystal. For the EPR measurements, a sample near the radial center, where the concentration of vacancy defects in the crystal boule had the highest value, was used. In addition, the out-of-phase spectra, and in-phase absorption spectra at a low microwave power are presented. These spectra are effective for the detection of defects with long relaxation times. The principle of EPR, EPR measurements in the dark and under illumination, the saturation phenomenon, out-of-phase spectra observation, and the sample preparation procedures are described in section 2. The EPR measurement results of this study are described in section 3. In section 4, the concentration of vacancy defects is estimated based on the EPR observations in the dark and under illumination, and previously reported PAS results and the EPR results are summarized. Finally, the paper is concluded in section 5.

2. Measurement principle and sample preparation

In this section, the principle of EPR, EPR measurements in the dark and under illumination, the saturation phenomenon, out-of-phase spectra observation, and the sample preparation procedures are described.

2.1. Principle of EPR

EPR is a spectroscopic tool for detecting unpaired electrons present in a substance. When an external magnetic field is applied to a sample that includes unpaired electrons, Zeeman splitting occurs in the spin eigenlevels of these electrons. Denoting the direction of the external magnetic field as the z direction, the magnetic interaction between the magnetic moment of an electron and the external magnetic field is represented by the Hamiltonian $\mathcal{H} = g\mu_B B S_z$. Here g is a dimensionless constant called the gyromagnetic factor (g factor), which takes the value of $g_e = 2.002\,319\ldots$ for a free electron, μ_B is the Bohr magneton, B is the magnitude of the external magnetic field, and S_z is the z component of the electron spin operator. There are two allowed orientations for the electron spin, namely, parallel or antiparallel to the external magnetic field. The orientation is specified by the electron spin quantum number m_s, which takes the value of either $-1/2$ or $+1/2$.

A magnetic-dipole transition between the Zeeman-split eigenlevels occurs when the unpaired electrons are irradiated by microwave radiation with an oscillating magnetic field perpendicular to the external magnetic field under the resonant condition

$$h\nu = g\mu_B B, \tag{1}$$

where h is the Planck constant and ν is the frequency of the microwave. This transition causes the absorption of the microwave and is called EPR.

Continuous EPR absorption is observed, when the population of the lower energy eigenlevel ($m_s = -1/2$) is larger than

that of the higher energy eigenlevel ($m_s = +1/2$). Such a population imbalance is maintained via spin–lattice relaxation, in which the absorbed energy of the spin system is dissipated via lattice vibrations (i.e., phonons).

In thermal equilibrium, the population ratio of the two spin eigenlevels ($m_s = -1/2$ and $m_s = +1/2$) approaches $\exp\left(g\mu_B B/kT\right)$ due to the Boltzmann distribution, where k is the Boltzmann constant and T is the absolute temperature. This ratio is approximately given by $(1 + g\mu_B B/kT)$ when the magnitude of the Zeeman splitting is sufficiently small compared to the thermal energy ($g\mu_B B \ll kT$). This condition is satisfied in this study. Thus, if the total number of spins in a sample is N, the number of spins in the two eigenstates are $\left(N/2\right)\left[1 \pm \left(g\mu_B B/2kT\right)\right]$ for $m_s = \mp 1/2$, respectively.

The magnetic moment of each unpaired electron takes the value of $\pm g\mu_B/2$ for $m_s = \mp 1/2$. Therefore, the net magnetization of a sample with N unpaired electrons in thermal equilibrium is given by $\left(+g\mu_B/2\right)\left(N/2\right)\left[1 + \left(g\mu_B B/2kT\right)\right] + \left(-g\mu_B/2\right)\left(N/2\right)\left[1 - \left(g\mu_B B/2kT\right)\right] = Ng^2{\mu_B}^2 B/\left(4kT\right)$. The net magnetization of the sample is proportional to N and inversely proportional to T.

The number of EPR-active defects (i.e., defects with unpaired electrons) in a sample can be quantitatively determined by comparing its EPR signal intensity with that of a reference sample with a known number of unpaired electrons. In general, the EPR absorption intensity for each defect (area of EPR absorption peak) is proportional to the number of unpaired electrons in the defect when the EPR measurements are carried out in the absence of saturation phenomenon (section 2.3). The number of a given type of defect X in the test sample, n_X, is given by

$$n_X = f\left(\frac{A_X}{A_R}\right)\left(\frac{T_X}{T_R}\right)n_R, \tag{2}$$

where n_R is the number of unpaired electrons in the reference sample, $\left(A_X/A_R\right)$ is the ratio of the observed EPR absorption intensities in the test and reference samples, $\left(T_X/T_R\right)$ is the ratio of the absolute temperatures of the test and reference samples, and f is a correction coefficient to account for the displacement of the sample position (or sample size) from the pin-point central position of the microwave resonator used in the study. The defect concentration is determined in cm^{-3} when the above number is divided by the sample volume.

In addition to the defect concentration, the types of defects present are reflected in the measured g factors. The g factor of a defect in a semiconductor is generally dependent on the direction of the external magnetic field. The majority of defects in silicon exhibit anisotropic g factors that can be used to identify the type of each individual defect.

2.2. EPR measurements in the dark and under illumination

EPR measurements were performed using a Bruker E500 X-band spectrometer equipped with a super-sensitive microwave ER 4122SHQ resonator (resonator Q value $\sim$ 12 000) and an Oxford ESR900 He-flow cryostat. The microwave frequency ν was stabilized at 9.445 GHz, and the external magnetic field B was swept from 333 mT to 342 mT. Copper(II) sulfate pentahydrate ($CuSO_4 \cdot 5H_2O$) with a mass of 12.53 mg was used as the reference sample for quantitative determination.

To improve the detection sensitivity, a lock-in amplifier and a magnetic field modulation technique were employed in the EPR spectrometer. In the magnetic field modulation technique, the differential change in the EPR absorption synchronized with the magnetic field modulation is measured to provide the first derivative of the absorption spectra. In this study, the modulation frequency and amplitude were set to 100 kHz and 0.1 mT, respectively. The EPR absorption peak can be obtained by integrating the measured EPR signal. The lock-in amplifier typically monitors the in-phase EPR signals that are synchronized exactly with the modulation of the magnetic field. In the absence of saturation phenomenon (section 2.3), the in-phase EPR signal offers the maximum detection sensitivity. In addition to conventional in-phase measurements, we also adopt an out-of-phase EPR detection for EPR signals under saturation, as explained in the next subsection.

The EPR measurements were carried out at 20 K, unless otherwise stated. Performing the measurements at lower temperatures drastically increases the population difference between the two spin levels and enhances the EPR absorption intensities. Furthermore, the dielectric loss of the microwave excitation is drastically reduced at lower temperatures, which further improves the detection sensitivity. However, such temperatures can also increase the spin relaxation time of unpaired electrons, which leads to the saturation phenomenon. The saturation phenomenon, which is discussed in the next subsection, needs to be considered in the measurements.

We performed EPR measurements both in the dark and under band-gap illumination (100 W halogen white light). Under illumination, EPR-inactive defects (defects without unpaired electrons) can be converted into EPR-active defects through the capture of photo-excited carriers. However, because the photoinduced conversion rate for each type of defect is unknown, the EPR absorption under illumination provides only the lower limit for the defect concentration.

A quartz glass rod used for introducing the sample into the microwave resonator was also used as a light guide for the halogen light. The intensity of the halogen light was adjusted to maximize the intensity of the EPR signals from the defects.

Anisotropic and high-intensity cyclotron resonance signals [11] were obtained in the EPR measurements performed at around 4 K in magnetic fields ranging from 52 mT to 185 mT. This indicates that the illumination generated a large number of electron–hole pairs in the silicon crystal in this study.

2.3. Saturation phenomenon and out-of-phase EPR observation

To observe EPR absorption continuously, spin relaxation processes are required to dissipate the Zeeman energy of the unpaired electrons as lattice vibrations. When the relaxation processes are not sufficiently activated, the continuous EPR absorption is decreased with increasing microwave power,

and eventually approaches zero. This is called the saturation phenomenon.

When saturation occurs, the line shape of the EPR absorption peak $Y(B)$ is given by [12]

$$Y(B) = \frac{sY_0}{1 + s(B - B_0)^2\gamma^2{T_2}^2}, \tag{3}$$

where s is the saturation coefficient, Y_0 is the amplitude of the EPR absorption at the center of the absorption peak without saturation, B_0 is the magnetic field at the center of the absorption peak, γ is the electron magnetic rotation ratio ($\gamma = g_e\mu_B/\hbar$), and T_2 is the spin–spin relaxation time. The saturation coefficient s is given by

$$s = \frac{1}{1 + \gamma^2{B_1}^2T_1T_2}, \tag{4}$$

where B_1 is the amplitude of the microwave magnetic field for exciting unpaired electrons, and T_1 is the spin–lattice relaxation time, which is larger than T_2. The saturation phenomenon occurs when $\gamma^2{B_1}^2T_1T_2 \gg 1$ and s approaches zero.

Equation (3) implies that the amplitude of the EPR absorption peak is proportional to s, and its line width is proportional to $s^{-1/2}$. As the extent of saturation increases, the line shape of the EPR absorption peak becomes increasingly broad, and the peak amplitude increasingly weak until EPR absorption finally disappears. Such situations may occur more frequently at lower temperatures because the spin–lattice relaxation time T_1 of every defect (and hence also T_2) becomes longer at lower temperatures, owing to the lack of phonons. Therefore, at lower temperatures, some of the EPR defect signals are suppressed because of the saturation phenomenon.

To detect such EPR signals with long relaxation times, an out-of-phase detection technique is conventionally used in which the EPR spectra are measured with the lock-in-detection phase shifted from 0° (in-phase) to 90° (out-of-phase) [13, 14]. The saturated signals are not synchronized with the magnetic-field modulation and thus appear as delayed signals. This setup is very useful for maximizing the delayed signals in the lock-in-detection system. The simultaneous application of excess microwave power and/or a rapid field modulation/sweep can facilitate out-of-phase detection because the saturation phenomenon is enhanced in such setups. Accordingly, in this EPR study, we adopted the so-called rapid passage method, in which a combination of out-of-phase (90° phase) detection, excess microwave power, and twice the field modulation rate (100 kHz → 200 kHz) was used. This measurement technique can selectively focus on EPR signals with long relaxation times. When the EPR spectra are observed in this way, each EPR signal shows a lineshape similar to an absorption peak.

2.4. Sample preparation

The shape of the silicon-28 single-crystal sample used in this study is almost the same as those used in previous studies [9, 10]. The sample is a solid cuboid with the dimensions of 1.8 mm × 3.4 mm × 10.0 mm. The 1.8 mm-long, 3.4 mm-long, and 10.0 mm-long edges are along the [011], [100], and $[0\bar{1}1]$ crystal orientations, respectively. Figure 1 shows the arrangement of the crystal orientation of the sample and the direction of the external magnetic field B applied to the sample.

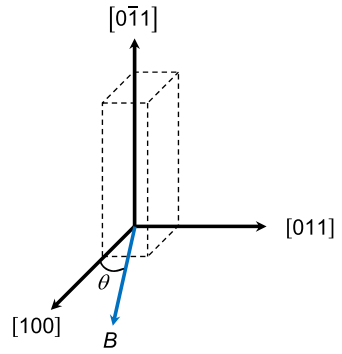

Figure 1. Crystal orientation of the sample and the direction of the applied external magnetic field B. The dotted line shows the outline of the sample. The external magnetic field B was applied perpendicular to the $[0\bar{1}1]$ crystal orientation. The angle θ is the angle between the external magnetic field B and the [100] crystal orientation.

This sample was cut from crystal boule Si28–23Pr11, which is a silicon-28 single crystal produced by Physikalisch-Technische Bundesanstalt (PTB) in 2015. Two 1 kg spheres, Si28kg01a and Si28kg01b, were fabricated from this crystal and used for the determination of the Avogadro constant and the realization experiments of the kilogram [15].

The sample used in this study was located 115 mm away from the seed and 2.5 mm from the radial center of crystal boule Si28–23Pr11. The sample was located near the radial center of the crystal boule where the defect concentration would be higher than that in the surrounding areas if vacancy defects exist in the boule [16]. Therefore, the sample used in this study is advantageous for the detection of the small number of vacancy defects in the crystal boule. Table 1 summarizes the locations of the silicon-28 crystal samples measured using EPR so far. The samples measured before this study were located more than 15 mm away from the radial center.

The sample surfaces were first mirror polished, and a layer with a thickness of about 2 μm was removed by etching with tetramethylammonium hydroxide (TMAH) solution. This eliminated the signals from mechanical damage defects on the surface ($Si_3 \equiv Si\bullet$, where the lines denote chemical bonds and the dot denotes an unpaired electron) which would otherwise overwhelm the signals from vacancy defects. After etching, the sample was placed in air at room temperature, and a natural oxide film was formed on the sample surface.

The mass of the sample is 139.2413(10) mg, and the volume of the sample calculated based on the crystal density [15] is 0.060 016(4) cm^3. The geometric surface area of the sample calculated from its dimensions is 1.16(2) cm^2, which consists of the surface area of 0.36(1) cm^2 from the Si(100) surfaces and the surface area of 0.80(1) cm^2 from the Si(110) surfaces. To introduce the sample into the cavity resonator of the EPR instrument, the sample was mounted on one end of a quartz glass rod with a length of 250 mm and diameter of 4 mm.

Table 1. The location of the samples in the crystal boules measured by EPR so far[a].

Crystal name	Sample region	Axial distance from seed/mm	Radial distance from center/mm	Reference
Si28–10Pr11	9.R1	∼420	35.0	[9]
Si28–10Pr11	9.R1	∼420	15.3	[10]
Si28–23Pr11	M.R2	∼115	18.8	[10]
Si28–23Pr11	M.R2	∼115	2.5	This study

[a]The Si28–10Pr11 crystal is also called the AVO28 crystal. Two 1 kg spheres, AVO28-S5c and AVO28-S8c, were produced from this crystal [17]. Two 1 kg spheres, Si28kg01a and Si28kg01b, were produced from the Si28–23Pr11 crystal [15].

3. Experimental results

EPR spectra were obtained under various conditions to detect vacancy defects in the silicon-28 crystal sample. We measured (i) the in-phase and out-of-phase spectra under illumination, (ii) the in-phase and out-of-phase spectra in the dark, and (iii) the in-phase spectra at low microwave power, as described in the following three subsections.

3.1. In-phase and out-of-phase EPR spectra under illumination

To search for vacancy defects in the sample, the in-phase and out-of-phase EPR spectra were obtained under illumination, as shown in figure 2. Measurements were carried out at the microwave frequency of $\nu = 9.445$ GHz with the microwave power of $p = 2$ mW. The out-of-phase EPR spectra can reveal defects that are difficult to detect from the in-phase spectra because of the saturation phenomenon.

To identify the type of defects, the EPR measurements were performed at the four different angles of $\theta = 0°$, 30°, 60°, and 90°. Each spectrum was obtained as the average of 20 scans performed over 30 min. The rotation of the sample resulted in slight fluctuations in the Q factor of the microwave resonator and therefore, fluctuations in the signal intensities, as shown in figure 2. The highest Q factor was obtained at $\theta = 0°$, at which the highest detection sensitivity was obtained. Therefore, we quantified the impurity and defect concentrations at $\theta = 0°$.

Two isotropic signals with the same intensity were observed in the first-derivative in-phase EPR spectra. Their mean position corresponds to the g factor of 1.9989, and their splitting width is 4.2 mT. The signals are consistent with a doublet signal of the phosphorus donors ($Si_4 \equiv P\bullet$, where '•' denotes an unpaired electron) in silicon [18]. The signal splitting is attributed to the hyperfine interaction between an unpaired electron and a ^{31}P nuclear spin ($I = 1/2$). Based on the absorption intensity, the concentration of phosphorus impurities with unpaired electrons was determined to be $3.4(5) \times 10^{12}$ cm^{-3} under illumination.

In addition, anisotropic signals with g factors ranging from 2.0021 to 2.0095 were observed. These angular-dependent signals arose from dangling bonds at the Si/SiO_2 interface ($Si_3 \equiv Si\bullet$, the so-called P_{b0} centers). This identification is based on the similarity of the observed g factors to those of the P_{b0} centers that predominantly form at the Si/SiO_2 interface at low oxidation temperatures (principal g factors of $g_Z = g_{\parallel} = 2.0018$ and $g_X = g_Y = g_{\perp} = 2.0082$ [19, 20]). The observed g factor of the P_{b0} center corresponds to the $g_{\parallel}$ ($g_{\perp}$) value when the dangling bond orbital is parallel to (perpendicular to) the external magnetic field. Figure 3 shows the angular dependence of the P_{b0} center. The points indicate the positions obtained from the out-of-phase spectra under illumination. These positions are in good agreement with the lines simulated from the above principal g factors.

The areal density of dangling bonds with unpaired electrons (P_{b0} centers) under illumination was evaluated to be $0.9(1) \times 10^{12}$ cm^{-2} based on the absorption intensity in the in-phase spectra. Because the P_{b0} centers exhibited more saturation behavior than the phosphorus donors, they appeared strongly in the out-of-phase spectra.

3.2. In-phase and out-of-phase EPR spectra in the dark

Following the previous section, the in-phase and out-of-phase EPR spectra were obtained in the dark. The purpose of these measurements is to quantitatively compare the EPR spectra obtained under illumination and in the dark to reveal the presence of defects in the sample that are otherwise invisible. In the previous section, we described the observation of EPR signals from phosphorus donors. If the sample includes compensation defects that can receive electrons from donors, the donor signal should be reduced in the dark because of the loss of unpaired electrons from the donors. The differential change in the donor signal indicates the amount of compensation defects (deep-level defects and acceptors). Because vacancy-type defects generally have deep energy levels, they act as compensation defects.

Figure 4 illustrates the electronic band structures in the dark (i.e., in thermal equilibrium) at cryogenic temperatures. The sample in this study includes phosphorus impurities that act as donors, as well as boron impurities and vacancy defects that act as acceptors. Because the phosphorus-donor level is very close to the conduction band edge (0.046 eV below the edge), nearly all the defect levels in the band gap act as acceptors when there is a sufficient amount of phosphorus donors.

In figure 4(a), where $n_D > n_A$, phosphorus donors that have lost an electron (indicated by an open circle) could not be observed by EPR because of the lack of an unpaired electron. Only $(n_D - n_A)$ of the phosphorus donors were observable. In contrast, in figure 4(b), where $n_D \leqslant n_A$, the phosphorus donors were not observed by EPR because all the phosphorus donors have lost an electron.

The measurements were carried out at the microwave frequency of $\nu = 9.445$ GHz with the microwave power of $p = 2$ mW. To identify the type of defects, measurements were

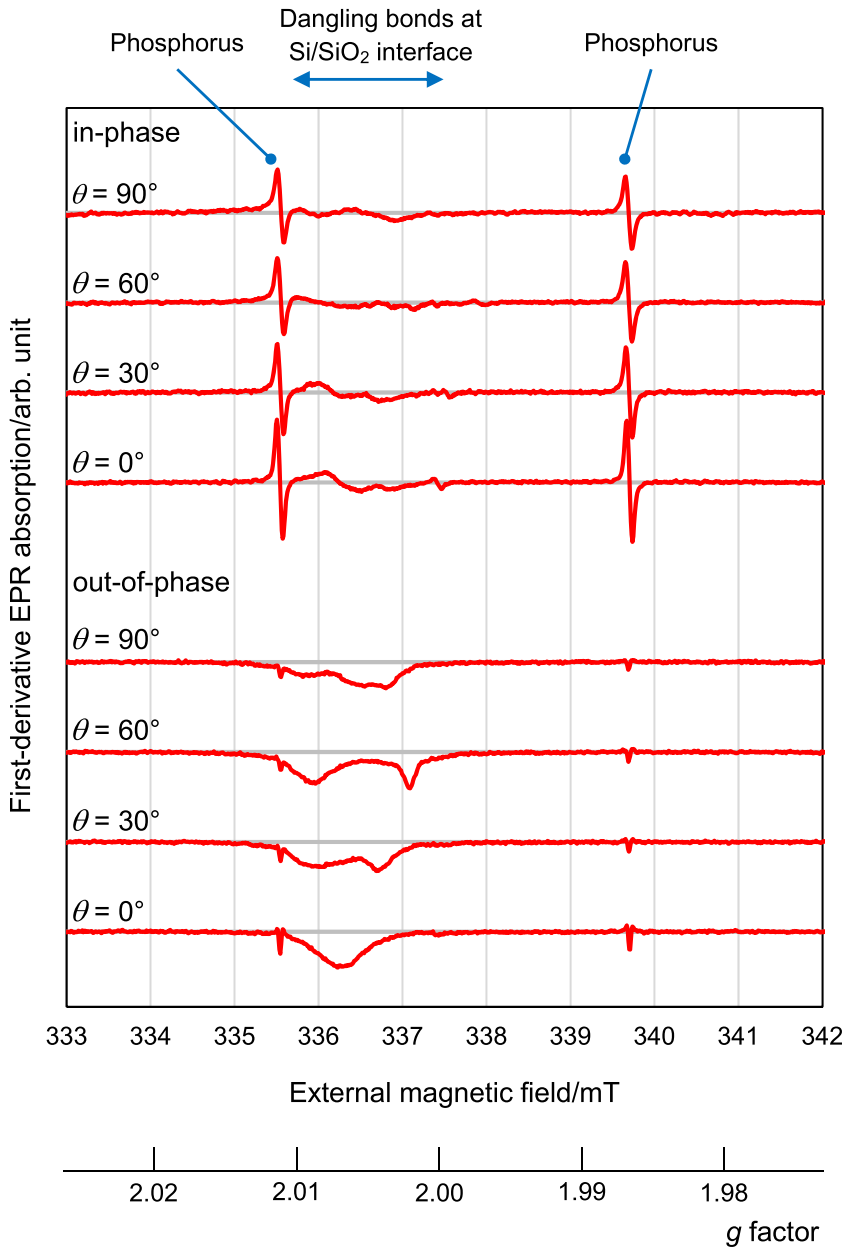

Figure 2. In-phase and out-of-phase EPR spectra under illumination. θ is the angle between the external magnetic field and the [100] crystalline axis. For each out-of-phase spectrum, a background spectrum from the quartz glass components of the EPR instrument was subtracted.

taken at the four different angles of $\theta = 0°$, 30°, 60°, and 90°. The measurement results are shown in figure 5. Each spectrum is the average of 20 scans performed over 30 min.

In the in-phase spectra, two isotropic signals from the phosphorus donors split by the hyperfine interaction were observed, similar to the measurements under illumination. Based on the intensity of these signals, the concentration of phosphorus impurities with unpaired electrons in the dark was determined to be $2.3(3) \times 10^{12}$ cm^{-3}. This result clearly demonstrates that the present sample satisfied the case shown in figure 4(a); namely, the concentration of phosphorus impurities acting as donors was larger than the sum of the concentrations of boron acceptors and vacancy defects acting as acceptors.

In addition to the phosphorus donors, weak EPR signals from the P_{b0} centers were observed, similar to the measurements under illumination. Based on the signal intensity, the dangling-bond areal density at the Si/SiO_2 interface in the dark was evaluated to be $0.4(1) \times 10^{12}$ cm^{-2}.

3.3. In-phase EPR spectra with low microwave power

In-phase EPR spectra were also obtained at the microwave frequency of $\nu = 9.445$ GHz with the low microwave power of $p = 0.002$ mW under illumination and in the dark to investigate the defects in the sample. Under this condition of a small microwave field amplitude B_1, the magnitude of $\gamma^2 {B_1}^2 T_1 T_2$ was sufficiently small to avoid the saturation phenomenon, even when the relaxation times of the

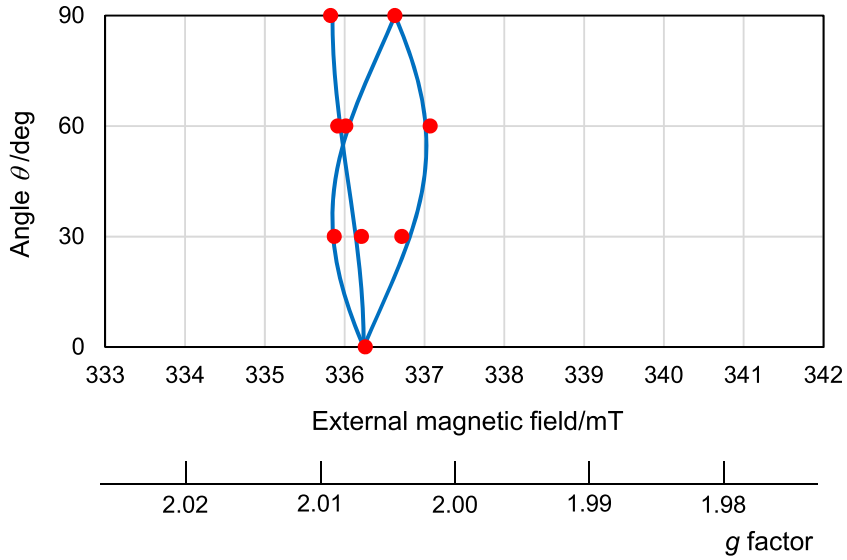

Figure 3. EPR signal positions of the dangling bonds at the Si/SiO_2 interface (P_{b0} centers). The points denote the positions obtained from the out-of-phase spectra under illumination. The lines are simulations with the principal g factors of $g_Z = g_{\parallel} = 2.0024$ and $g_X = g_Y = g_{\perp} = 2.0094$. The angle θ on the vertical axis is the angle between the external magnetic field B and the [100] crystal orientation. To convert the g factor to the magnitude of the external magnetic field B, the microwave frequency of $\nu = 9.445$ GHz was used. Owing to the rotational symmetry of the silicon crystal, up to 12 absorption peaks may appear depending on the direction of the external magnetic field.

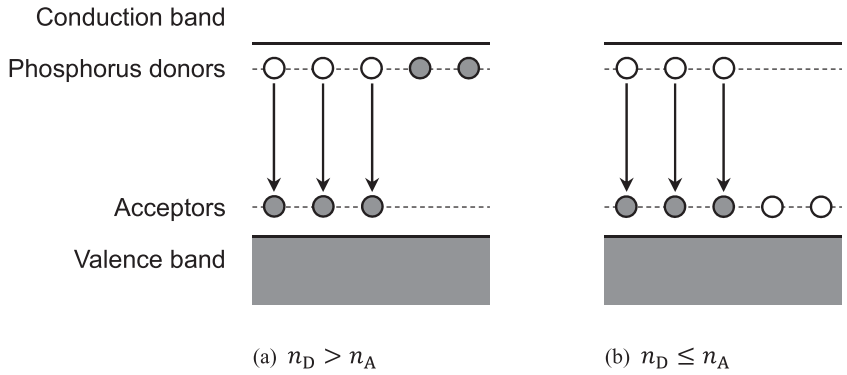

Figure 4. Electronic band structures of silicon in the dark at cryogenic temperatures with (a) $n_D > n_A$ and (b) $n_D \leqslant n_A$, where n_D is the donor concentration and n_A is the acceptor concentration. The gray circles indicate electrons. The electrons occupy the energy levels from the lowest level to the upper levels in sequence in the dark at cryogenic temperatures. Because the centers observable by EPR must have unpaired electrons, phosphorus donors are partially EPR-active in case (a), and all of them are EPR-inactive in case (b) in the dark at cryogenic temperatures.

unpaired electrons localized at defects became longer at low temperatures.

The measurement results are shown in figure 6. The measurements were performed at $\theta = 0°$. Each spectrum is the average of 500 scans performed over a 12 h period. The measurements at low microwave power required a larger number of scans to improve the signal-to-noise ratio. Similar to the measurements under $p = 2$ mW shown in the previous subsections, only phosphorus donors and P_{b0} centers were detected (figure 6).

Tables 2(a) and (b) summarize the measurement results of the phosphorus donor concentration and dangling bond areal density at the Si/SiO_2 interface based on the in-phase EPR spectra shown in subsections 3.1–3.3.

The phosphorus donor concentration and the dangling bond areal density were higher under illumination than in the dark, as shown in table 2(a). This is because these EPR centers were partially compensated (lost unpaired electrons) in the dark both in the bulk and at the surfaces. In contrast, the EPR centers were converted into EPR-active states under illumination when they received unpaired electrons via the photoexcitation of a large number of electron–hole pairs in the silicon crystal. As a result, the phosphorus donors underwent the transition $Si_4 \equiv P + \bullet \rightarrow Si_4 \equiv P\bullet$ ('•' denotes an unpaired electron) in the bulk, and the P_{b0} centers underwent the transition $Si_3 \equiv Si + \bullet \rightarrow Si_3 \equiv Si\bullet$ at the Si/SiO_2 interfaces on the sample surface.

A clear signature of the saturation behavior was found for the P_{b0} centers. Their concentration was reduced to approximately half under $p = 2$ mW, as shown in table 2(b). This indicates that the deep-level defects, such as P_{b0} centers, exhibited relatively long relaxation times. By analogy with the P_{b0}

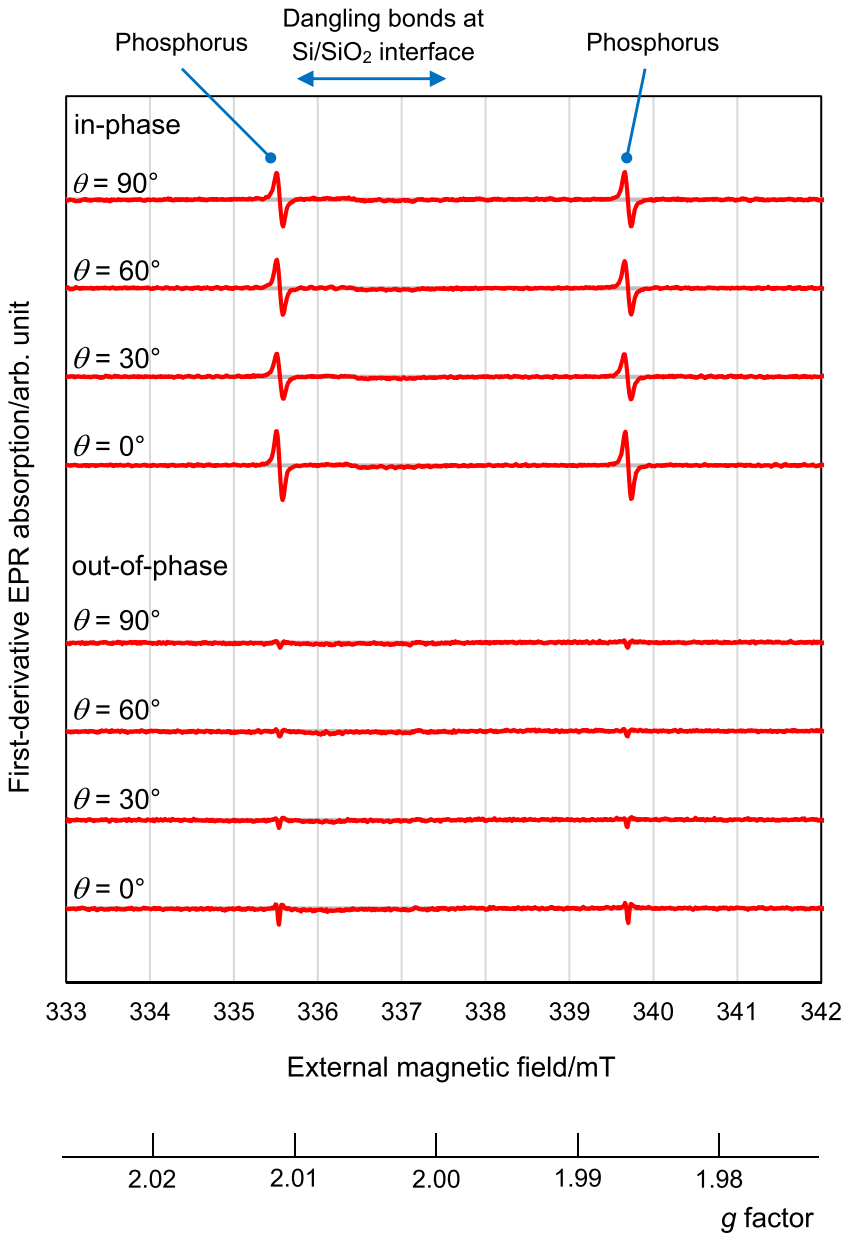

Figure 5. In-phase and out-of-phase EPR spectra in the dark. θ is the angle between the external magnetic field and the [100] crystalline axis. For each out-of-phase spectrum, the background spectrum from the quartz glass components of the EPR instrument was subtracted. To quantify the concentrations of impurities and defects, the in-phase spectrum measured at $\theta = 0^\circ$ was used.

centers, the vacancy defects may also have long relaxation times. However, the EPR measurements that focused on such slow-relaxation centers (the out-of-phase spectra shown in figures 2 and 5, and the low-power EPR spectra shown in figure 6) did not find any EPR signals from the nine types of EPR-active vacancy defects, namely, V^+, V^-, $V_2{}^+$, $V_2{}^-$, $V_3{}^-$, $V_4{}^-$, $V_5{}^-$, $(VO)^-$, and $(VP)^0$ [21]. Therefore, we concluded that the concentration of each of these defects was below the detection sensitivity, which was estimated to be approximately 1×10^{12} cm^{-3}, similar to previous EPR studies [9, 10].

4. Discussion

4.1. Concentration of electrically-active vacancy defects

The EPR spectra obtained under various conditions, namely, the (i) in-phase and out-of-phase spectra under illumination, (ii) in-phase and out-of-phase spectra in the dark, and (iii) in-phase spectra at a low microwave power, were described in the previous section. In every condition, only EPR signals from the phosphorous donors in the bulk and the P_{b0} centers at the Si/SiO$_2$ interface were detected. No other signals above the detection sensitivity of this study (around 1×10^{12} cm^{-3};

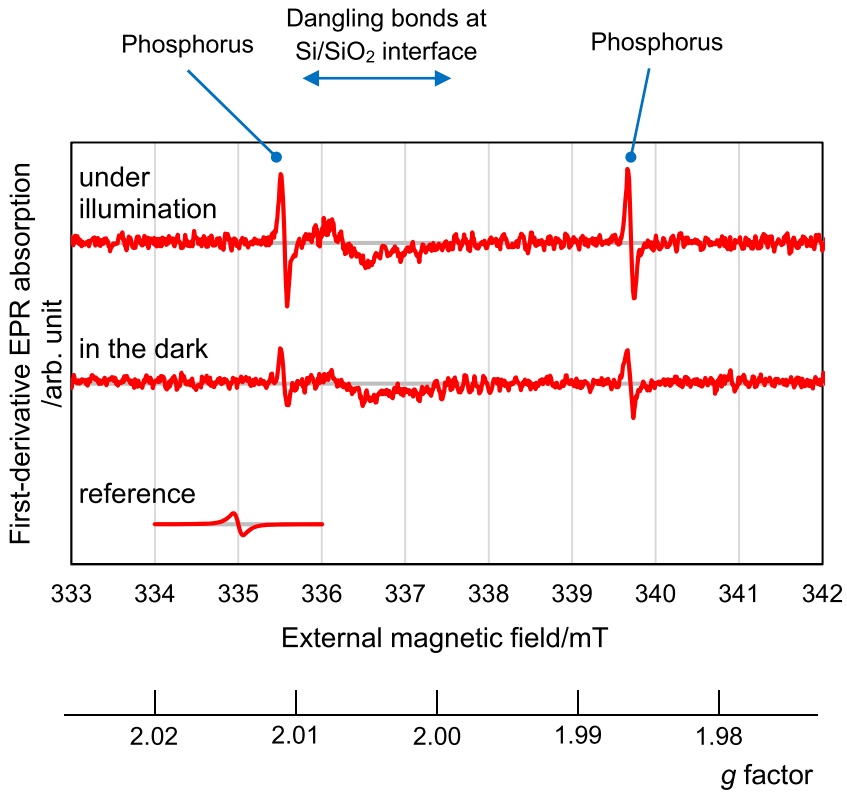

Figure 6. In-phase EPR spectra under illumination and in the dark obtained at low microwave power. The angle between the external magnetic field and the [100] crystalline axis was set to $\theta = 0°$. A reference EPR signal with an electron spin concentration of 1×10^{12} cm^{-3} and a half width at half maximum of 0.1 mT is shown.

Table 2. (a) Concentration of observed EPR-active phosphorus donors. (b) Areal density of observed EPR-active dangling bonds (P_{b0} centers).

(a)

Subsection	Observation conditions	Phosphorus donor concentration/ (10^{12} cm^{-3})	Difference between under illumination and in the dark/(10^{12} cm^{-3})
3.1	$p = 2$ mW, under illumination, in-phase	3.4(5)	1.1(6)
3.2	$p = 2$ mW, in the dark, in-phase	2.3(3)	
3.3	$p = 0.002$ mW, under illumination, in-phase	3.2(4)	1.6(5)
3.3	$p = 0.002$ mW, in the dark, in-phase	1.6(2)	

(b)

Subsection	Observation conditions	Dangling bond areal density/(10^{12} cm^{-2})
3.1	$p = 2$ mW, under illumination, in-phase	0.9(1)
3.2	$p = 2$ mW, in the dark, in-phase	0.4(1)
3.3	$p = 0.002$ mW, under illumination, in-phase	1.7(2)
3.3	$p = 0.002$ mW, in the dark, in-phase	0.8(1)

see reference EPR signal with a spin concentration of 1×10^{12} cm^{-3} in figure 6) were detected. We confirmed that there was no detectable vacancy defect signals in the sample, including those from the nine types of EPR-active vacancy defects [V^+, V^-, $V_2{}^+$, $V_2{}^-$, $V_3{}^-$, $V_4{}^-$, $V_5{}^-$, $(VO)^-$, and $(VP)^0$]. These defects exhibit anisotropic EPR signals with principal g factors ranging from 1.9989 to 2.0151, as established in previous EPR studies [21].

Here, we focus on the bulk region. The concentration of phosphorus donors observed under illumination was higher than that in the dark. The former was found to be between 3.2(4) $\times$ 10^{12} cm^{-3} and 3.4(5) $\times$ 10^{12} cm^{-3}, as

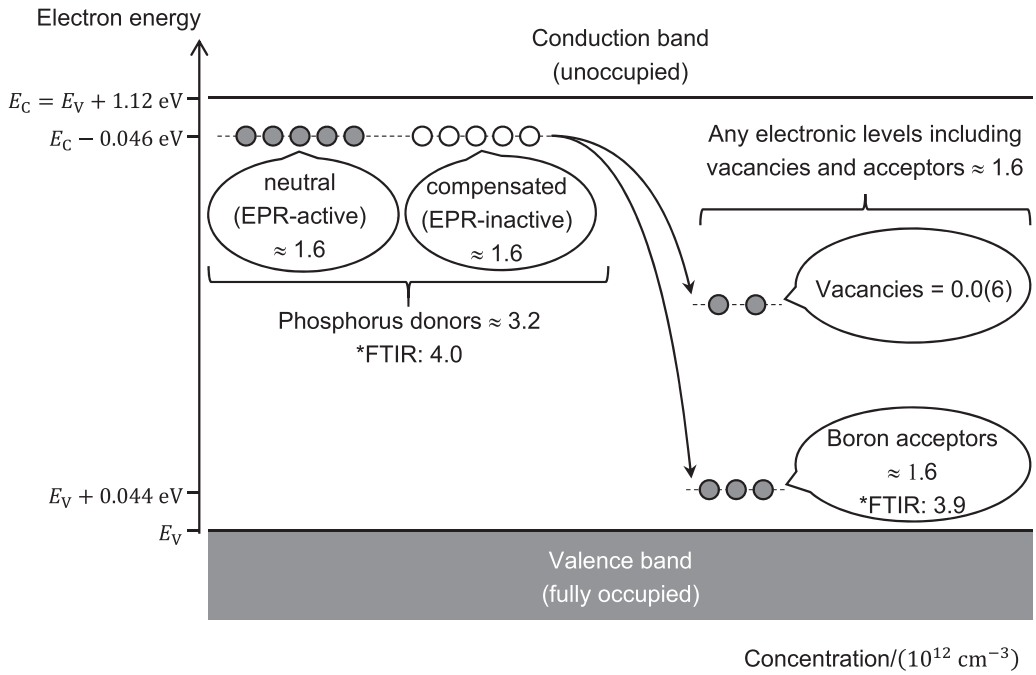

Figure 7. Summary of concentrations of phosphorus donors, boron acceptors, and all other electronic levels including vacancy defects in the sample. The gray circles indicate electrons. The values of the bandgap and the phosphorus donor and boron acceptor energies were taken from reference [22]. FTIR values were taken from reference [15].

Table 3. Summary of the measured vacancy defect concentrations.

Measurement method	Crystal	Vacancy defect concentration/ (10^{14} cm^{-3})	Corresponding mass deficit for a 1 kg sphere/μg	Reference
PAS	Isotopically natural silicon FZ crystal	1–4, quantified as monovacancy defects	2–8	[7]
PAS	Silicon-28 FZ crystal	3.3(1.1), quantified as monovacancy defects	6.6(2.2)	[8]
EPR	Silicon-28 FZ crystal	0.000(6)	0.0(1)	This study

shown in table 2(a), which agrees well with the value of 4.0(1.0) × 10^{12} cm^{-3} measured using Fourier-transform infrared spectroscopy (FTIR) on sample M.2 close to the sample of this study [15] within their combined uncertainties.

The difference in the phosphorus donor concentration under illumination and in the dark was estimated to be 1.1(6) × 10^{12} cm^{-3} to 1.6(5) × 10^{12} cm^{-3} (see table 2(a)). This difference reflects the total amount of electronic levels in the band gap that were deeper than the phosphorus donor level (0.046 eV below the conduction band edge) and hence acted as acceptors. Therefore, the concentration of electrically active vacancy defects with energy levels in the band gap was determined to be at most the differential concentration ($\leqslant$1.6 × 10^{12} cm^{-3}) indicated above. In addition, the concentration of boron impurities is included in this upper limit.

As mentioned above, sample M.2 from crystal boule Si28–23Pr11, which was located close to the sample in this study, was measured using FTIR [15]. The boron impurity concentration was measured to be 3.9(5) × 10^{12} cm^{-3}. Because this concentration is larger than the upper limit of 1.6 × 10^{12} cm^{-3} obtained in our measurements, we can conclude that our result is nearly fully due to boron impurities. Consequently, we estimate the contribution of electrically active vacancy defects is zero, i.e., 0.0 × 10^{12} cm^{-3}. We then estimate its standard uncertainty to be 0.6 × 10^{12} cm^{-3}, assuming a uniform distribution with a half-width of 1 × 10^{12} cm^{-3}, the magnitude of which is the detection sensitivity of this study. We emphasize that this estimation is consistent with the absence of any vacancy defect signals, as noted earlier.

Figure 7 shows a summary of the concentrations of phosphorus donors, boron acceptors, and all other electronic levels, including vacancy defects in the sample, based on observations under illumination and in the dark at the microwave power of $p = 0.002$ mW. The phosphorus donors were partially compensated (lost their electrons) by electronic levels deeper than the phosphorus donor levels. The concentration of such deep levels was at most 1.6 × 10^{12} cm^{-3}. Most of these levels were contributed by boron acceptors (estimated to be nearly 1.6 × 10^{12} cm^{-3}). Finally, the concentration of electrically active vacancy defects was estimated to be smaller than 0.0(6) × 10^{12} cm^{-3}.

4.2. Summary of PAS and EPR results

In the realization of the kilogram by the XRCD method, the vacancy defect concentration measured by PAS is currently employed for the mass deficit correction. To verify the reliability of this mass defect correction, this study used EPR, an independent method different from PAS, to measure the vacancy defect concentration in silicon-28 single crystal.

Table 3 summarizes the measurement results of the vacancy defect concentration by PAS and EPR for the realization of the kilogram by the XRCD method. In these measurements, silicon crystals grown using the floating zone (FZ) method were investigated.

In the PAS measurements, the average positron lifetime exceeded the bulk lifetime by only a few picoseconds, and the lifetime spectrum of the sample could not be decomposed consistently. Therefore, the type of vacancy defect has not been identified, and its concentration has not been directly determined. Details are given in the appendix of this study. The vacancy defect concentration, estimated from the increase in the average positron lifetime at cryogenic temperatures, was at the 10^{14} cm^{-3} level in monovacancy equivalent.

In contrast, the EPR measurements in this study did not detect any vacancy defects, including the nine types of EPR-active vacancy defects. In addition, EPR signals from phosphorus impurities that acted as donors at a cryogenic temperature in the dark were observed, which indicates that the concentration of electrically active vacancy defects in the sample was $0.0(6) \times 10^{12}$ cm^{-3}, as described in the previous subsection. The mass deficit correction for a 1 kg silicon sphere was evaluated to be 0.0(1) μg.

The number of atoms contained in a single-crystal silicon-28 sphere is counted by measuring its volume and lattice constant to realize the kilogram in the XRCD method, where the mass deficit corresponding to the vacancy defect concentration is subtracted. Therefore, if the EPR result of this study is adopted instead of the PAS result, the values reported from PTB and National Metrology Institute of Japan (NMIJ) using the XRCD method in the CCM.R-kg-P1 pilot study and CCM.M-K8.2019 key comparison would be corrected by +6.6 μg. The magnitude of this proposed correction is small compared to the uncertainties reported from PTB and NMIJ. In addition, their values after the correction remain consistent with the reference values in the two international comparisons.

One of the possible causes for the discrepancy between the PAS and EPR results could be that the vacancy defect concentration determined using EPR was an underestimated value. The properties of vacancy aggregates up to heptavacancy V_7 in silicon crystals have been studied using molecular dynamics simulations and molecular orbital methods [23]. The hexavacancy V_6, which has a ring configuration of vacancies, is electrically inactive because it has no deep levels in the band gap. If such ring-hexavacancy V_6 defects exist in silicon crystals, it is highly likely that they cannot be detected by EPR.

5. Conclusion

EPR spectra were observed under various conditions on a sample cut from the Si28–23Pr11 crystal boule, which was produced for experiments to realize the kilogram. A part close to the radial center of the crystal boule, which has a high concentration of vacancy defects if they exist, was chosen for the sample. We obtained the (i) in-phase and out-of-phase spectra under illumination, (ii) in-phase and out-of-phase spectra in the dark, and (iii) in-phase spectra at low microwave power. We draw the following conclusions from our measurement results:

(a) In the out-of-phase spectra and in-phase spectra at low microwave power, the signals from the dangling bonds at the Si/SiO_2 interface (P_{b0} centers), which showed saturation behavior at low temperatures, were observed with higher intensities. This indicates that even defects with long relaxation times can be detected with high sensitivity by measuring the out-of-phase spectra or in-phase spectra at low microwave power.

(b) EPR measurements were performed on a silicon-28 crystal. These measurements included measurements of the out-of-phase and in-phase spectra at low microwave power, which are useful for detecting defects with long relaxation times. However, only signals from phosphorus impurities in the sample and dangling bonds at the Si/SiO_2 interface (P_{b0} centers) were detected. Anisotropic signals from vacancy defects were not observed. Therefore, we conclude that the concentration of each of the nine types of EPR-active vacancy defects in the sample was below the detection sensitivity of our EPR measurement (approximately 1×10^{12} cm^{-3}).

(c) EPR signals from the phosphorus donors were observed in the dark at cryogenic temperatures, indicating that the concentration of phosphorus donors was higher than the total concentration of boron impurities and vacancy defects acting as acceptors. The concentration of the compensated phosphorus donors was estimated to be approximately 1.6×10^{12} cm^{-3}. Because most of the compensation was contributed by boron acceptors, the concentration of electrically active vacancy defects was estimated to be $0.0(6) \times 10^{12}$ cm^{-3}. The mass deficit correction for a 1 kg silicon sphere was evaluated to be 0.0(1) μg.

(d) Previously reported PAS results and EPR results in this study for the vacancy defect concentration were summarized. One of the possible causes for the discrepancy between the PAS and EPR results is that the PAS measurement did not identify the type of vacancy defect and did not directly determine the vacancy defect concentration. Another possible cause is the presence of electrically inactive V_6 hexavacancy defects, which have a ring configuration of vacancies and are unlikely to be detected by EPR.

Acknowledgments

This work was supported by JSPS KAKENHI Grant No. 17K05112. Some of the sample preparation processes were carried out in the Clean Room for Analog–Digital Superconductivity (CRAVITY) at the National Institute of Advanced Industrial Science and Technology (AIST) and MicroNano Open Innovation Center (MNOIC). The silicon-28 crystal cut from crystal boule Si28–23Pr11 was provided by the PTB based on an international cooperation between PTB and NMIJ in realization of the kilogram.

Appendix.

The measurement and analysis of the vacancy defect concentration in FZ silicon crystals using PAS was described in detail by Gebauer *et al* [7]. In that study, the average positron lifetime τ_{av} was observed because the lifetime spectra could not be consistently decomposed in a sample in which the average positron lifetime exceeded the bulk lifetime by only a few picoseconds. The average positron lifetime τ_{av} increased by approximately 1.5 ps when the temperature was decreased from 300 K to 20 K. This increase in the average positron lifetime was also detected after the sample was annealed at 500 °C for 1 h. Therefore, it was concluded that the positron trapping could not be explained by simple point defects (V, V_2, VO, and V_2O) with low thermal stability. Because the carrier concentration in the high-resistivity FZ crystal was only on the order of 10^{12} cm^{-3}, it was deduced that the detected vacancies with a concentration of 10^{14} cm^{-3} were electrically neutral. The PAS results were hence attributed to electrically neutral vacancy aggregates such as V_6 defects. In addition, the positron lifetime in an as-grown FZ-Si crystal was compared with that of the electron-irradiated crystals using the estimated monovacancy introduction rate of $\Sigma = 0.1$ cm^{-1}. It was concluded that the concentration of the monovacancy defects in the as-grown FZ-Si crystal would be between 1×10^{14} cm^{-3} and 4×10^{14} cm^{-3}.

The trapping rate of positrons into a specific type of vacancy defect κ_{vac}, the trapping coefficient specific to these vacancy defects μ_{vac}, and the concentration of the defects c_{vac} are related by

$$\kappa_{\mathrm{vac}} = \frac{1}{\tau_{\mathrm{bulk}}} \frac{(\tau_{\mathrm{av}} - \tau_{\mathrm{bulk}})}{(\tau_{\mathrm{vac}} - \tau_{\mathrm{av}})} = \mu_{\mathrm{vac}} c_{\mathrm{vac}}, \tag{A1}$$

where τ_{bulk} is the positron lifetime in the bulk and τ_{vac} is the positron lifetime of the vacancy defects.

In reviewing the paper by Gebauer *et al* [7], we found three unclarified issues that affected the mass deficit correction based on the number of vacancy defects measured using PAS:

(a) The type of vacancy defects was assumed to be electrically neutral V_6 defects. However, the trapping coefficient of $\mu_{\mathrm{vac}} = 10^{16}$ s^{-1} [24] for negatively charged monovacancy defects V^- at the temperature of 90 K was used to calculate the vacancy concentration c_{vac}. The use of the value of $\mu_{\mathrm{vac}} = 10^{16}$ s^{-1} is questionable because the trapping coefficient varies with the type and charge state of the defects. In particular, it was reported that the trapping coefficient of negatively charged defects is more than ten times larger than that of neutral defects [25].

(b) A computational study based on the superposition of the free-atomic densities and the three-dimensional solution of the positron Schrödinger equation showed that the positron lifetime in vacancy defects increases as a function of the vacancy size and rapidly saturates to the limit of 500 ps. The positron lifetime does not depend linearly on the vacancy defect size [26]. Therefore, if the PAS spectra are not decomposed and the size of the vacancy defects cannot be determined, the correction for the mass deficit cannot be calculated accurately in the XRCD method, in which the correction is given by the product of the size and concentration of the vacancy defects.

(c) First-principles calculations show that negative ions in semiconductors have a large positron trapping rate at low temperatures that is comparable to the positron trapping rate of vacancy defects [27]. In general, FZ silicon crystals contain non-negligible concentrations of boron impurities that are negatively charged at low temperatures with an electron density that is smaller than that of silicon atoms, that is, $\rho\left(\mathrm{B}^-\right)/\rho\,(\mathrm{Si}) = 6/14$. In the Si28–23Pr11 silicon-28 crystal, the concentration of boron impurities measured using FTIR ranged from 1.7×10^{12} cm^{-3} to 9.8×10^{12} cm^{-3} [15]. Therefore, at least a part of the increase in the average positron lifetime τ_{vac} with decreasing temperature can be attributed to positron trapping by boron impurities. The increase in the average positron lifetime does not necessarily indicate the presence of vacancy defects.

ORCID iDs

Shigeki Mizushima https://orcid.org/0000-0003-1276-1328
Takahide Umeda https://orcid.org/0000-0002-2584-4782

References

[1] Bureau International des Poids et Mesures 2018 *Proc. of the 26th Meeting of the General Conf. on Weights and Measures* (November 2018) pp 472–4 available on the BIPM website: www.bipm.org
[2] Consultative Committee for Mass and Related Quantities 2019 Mise en pratique for the definition of the kilogram in the SI in appendix 2 of the International System of Units (SI) 9th edn available on the BIPM website: www.bipm.org
[3] Stock M *et al* 2018 A comparison of future realizations of the kilogram *Metrologia* **55** T1
[4] Stock M *et al* 2020 Report on the CCM key comparison of kilogram realizations CCM.M-K8.2019 final report *Metrologia* **57** 07030
[5] Stock M and Davidson S 2020 Report on the calculation of the CCM consensus value for the kilogram 2020 available on the BIPM website: www.bipm.org
[6] Fujii K *et al* 2016 Realization of the kilogram by the XRCD method *Metrologia* **53** A19

[7] Gebauer J, Rudolf F, Polity A, Krause-Rehberg R, Martin J and Becker P 1999 On the sensitivity limit of positron annihilation: detection of vacancies in as-grown silicon *Appl. Phys.* A **68** 411–6
[8] Andreas B *et al* 2011 Counting the atoms in a ^{28}Si crystal for a new kilogram definition *Metrologia* **48** S1
[9] Mizushima S, Kuramoto N, Fujii K and Umeda T 2019 Electron paramagnetic resonance study on ^{28}Si single crystal for the future realization of the kilogram *IEEE Trans. Instrum. Meas.* **68** 1879–86
[10] Mizushima S, Kuramoto N and Umeda T 2021 Determination of defect concentrations in ^{28}Si crystals using EPR for the realization of the kilogram *IEEE Trans. Instrum. Meas.* **70** 1–6
[11] Dresselhaus G, Kip A F and Kittel C 1955 Cyclotron resonance of electrons and holes in silicon and germanium crystals *Phys. Rev.* **98** 368–84
[12] Poole C P Jr 1983 *Electron Spin Resonance: A Comprehensive Treatise on Experimental Techniques* 2nd edn (New York: Wiley-Interscience) pp 589–600
[13] Poole C P Jr 1983 *Electron Spin Resonance: A Comprehensive Treatise on Experimental Techniques* 2nd edn (New York: Wiley-Interscience) pp 627–32
[14] Harbridge J R, Rinard G A, Quine R W, Eaton S S and Eaton G R 2002 Enhanced signal intensities obtained by out-of-phase rapid-passage EPR for samples with long electron spin relaxation times *J. Magn. Reson.* **156** 41–51
[15] Bartl G *et al* 2017 A new ^{28}Si single crystal: counting the atoms for the new kilogram definition *Metrologia* **54** 693
[16] Abe T, Harada H and Chikawa J 1983 Swirl defects in float-zoned silicon crystals *Physica B+C* **116** 139–47
[17] Azuma Y *et al* 2015 Improved measurement results for the Avogadro constant using a ^{28}Si-enriched crystal *Metrologia* **52** 360
[18] Low W 1960 *Paramagnetic Resonance in Solids* (*Solid State Physics* vol 2) (New York: Academic) pp 177–9
[19] Stesmans A and Afanas'ev V V 1998 Electron spin resonance features of interface defects in thermal (100)Si/SiO_2 *J. Appl. Phys.* **83** 2449–57
[20] Keunen K, Stesmans A and Afanas'ev V V 2011 Inherent Si dangling bond defects at the thermal (110)Si/SiO_2 interface *Phys. Rev.* B **84** 085329
[21] Ammerlaan C A J, Bracht H, Haller E E, Murray R, Newman R C, Sauer R, Stolwijk N A, Weber J and Zulehner W 2002 Paramagnetic centers in silicon *Landolt–Börnstein Group III Condensed Matter* vol 41A2α (Berlin: Springer) pp 244–308
[22] Sze S M, Li Y and Ng K K 2021 *Physics of Semiconductor Devices* 4th edn (New York: Wiley) p 21
[23] Hastings J L, Estreicher S K and Fedders P A 1997 Vacancy aggregates in silicon *Phys. Rev.* B **56** 10215–20
[24] Mäkinen J, Corbel C, Hautojärvi P, Moser P and Pierre F 1989 Positron trapping at vacancies in electron-irradiated Si at low temperatures *Phys. Rev.* B **39** 10162–73
[25] Kawasuso A, Hasegawa M, Suezawa M, Yamaguchi S and Sumino K 1995 Charge state dependences of positron trapping rates associated with divacancies and vacancy–phosphorus pairs in Si *Japan J. Appl. Phys.* **34** 2197–206
[26] Puska M J and Corbel C 1988 Positron states in Si and GaAs *Phys. Rev.* B **38** 9874–80
[27] Puska M J, Corbel C and Nieminen R M 1990 Positron trapping in semiconductors *Phys. Rev.* B **41** 9980–93